High Temperature Superconductivity in Single-Unit-Cell-FeSe/$TiO_{2-\delta}$

LILI WANG, QI-KUN XUE
DEPARTMENT OF PHYSICS, TSINGHUA UNIVERSITY

ABSTRACT

Engineering of heterostructures is a vibrant frontier in realizing novel electronic states of matter. A recent breakthrough is that single unit-cell FeSe films grown on several $TiO_{2-\delta}$ terminated substrates, including $SrTiO_3$, $BaTiO_3$ and TiO_2, universally exhibit an enlarged superconducting gap up to 20 meV, nearly one order of magnitude larger than that of bulk FeSe. Consequently, the critical transition temperature (T_c) is significantly promoted to a value higher than 65 K, which is the highest T_c among all known Fe-based superconductors. Intensive experimental investigations indicate that two interface effects, i.e. interface charge transfer and interface electron-phonon coupling, contribute to the high temperature superconductivity therein. The FeSe/$TiO_{2-\delta}$ interface bears a strong resemblance to the built-in interface structures in cuprates and iron pnictides. Thus, the discovery of interface high temperature superconductivity in an FeSe/$TiO_{2-\delta}$ interface not only opens a new avenue for raising superconducting transition temperatures, but also sheds new light on understanding the mechanism of high temperature superconductivity in cuprates.

INTRODUCTION

Searching for superconducting materials with a high transition temperature (T_c) is one of the most exciting and challenging fields in physics and materials science. In more than 100 years since the discovery of superconducting behavior in mercury and tin [1], two families of high-T_c superconductors have been discovered, i.e. cuprates [2] and Fe-based superconductors [3]. They share similar sandwiched structures consisting of alternative superconducting layers (CuO_2 layer and FeAs layer for cuprates and iron pnictides, respectively) and charge reservoir layers, where the superconductivity occurs with charge transferred from the charge reservoir layers into the superconducting layers without chemical dopants and defects being introduced into the latter. The structural features and the corresponding interface doping mechanism, similar to modulation doping in the semiconductor superlattices of AlGaAs/GaAs [4], stimulated our interest in searching for high-temperature superconductivity (HTS) in a designed heterostructure. Along this direction, we artificially constructed heterostructure of superconducting films on semiconductor/oxidation substrates by using state-of-the-art molecular beam epitaxial growth, and studied the superconductivity therein by *in-situ* scanning tunneling microscopy/spectroscopy (STM/STS) and transport measurements. In 2012, we reported the STS observation of a superconducting gap of 20 meV, nearly one order of magnitude higher than that of bulk FeSe, in single unit cell (UC) FeSe films on $SrTiO_3$(STO)(001) substrates (denoted as FeSe/STO(001) hereafter) [5]. In last five years, several related heterostructures, such as FeSe/$BaTiO_3$(001) [6], FeSe/STO(110) [7, 8] and FeSe/TiO_2(001) [9, 10], are found to host similar HTS. These heterostructures share the same interface, i.e. directly bounded FeSe/$TiO_{2-\delta}$ interface, where the subscript δ marks oxygen vacancies in the interface TiO_2 layer. From the band structure point of view, it is reminiscent of the built-in multi-interfaces in cuprates (e.g. CuO_2/LaO) [11] and iron pnictides (e.g. FeAs/LaO) [12] superconductors. Here the FeSe and $TiO_{2-\delta}$ layers act as the electron transporting layer and charge reservoir layers, respectively. More strikingly, not only interface charge transfer but also interface enhanced electron-phonon (*e-ph*) coupling are experimentally revealed to play crucial roles [10, 13-19]. The interfacial effects and their contribution to the HTS are also theoretically supported [20-23], albeit the pairing mechanism of the HTS

at FeSe/$TiO_{2-\delta}$ interface remains obscure. The discovery of HTS at such artificially constructed heterostructures opens a new avenue for raising T_c and sheds new light on understanding the pairing mechanism of HTS.

Structure and superconductivity in 1UC-FeSe/$TiO_{2-\delta}$

The bulk β-phase FeSe is a superconductor with a maximum T_c of 9 K at ambient pressure [24]. One unit cell β-phase FeSe consists of two Se layers sandwiching a Fe layer with an in-plane lattice constant $a_0 = b_0 = 3.78$ Å and an out-of-plane lattice constant $c_0 = 5.50$ Å. The superconductivity in bulk FeSe is extremely sensitive to the stoichiometry, and the clean superconducting phase exists only in stoichiometric FeSe samples with minor Se deficiency [25]. So is the HTS in FeSe/$TiO_{2-\delta}$. Thus, we prepared epitaxial 1UC-FeSe films by co-evaporating Fe and Se under Se-rich conditions (typical flux ratio of ~ 1:10 to ensure the stoichiometry), and then did post-annealing to remove extra Se adatoms. The epitaxial 1UC-FeSe films on STO(001), STO(110), $BaTiO_3$(001) and TiO_2(001) (Anatase and Rutile) have uniform Se-terminated (001) surfaces (Fig. 1(a) and 1(b)), but their in-plane lattice constants depend on those of the $TiO_{2-\delta}$ layer, with which they are interfaced [5-9]. As summarized in Table 1, the in-plane lattice constants range from 6% compression to 6% expansion compared with bulk FeSe. However, all those 1UC-FeSe films exhibit similar superconducting gaps of 16-20 meV (somehow sample quality dependent) that close at 60-70 K (Table 1).

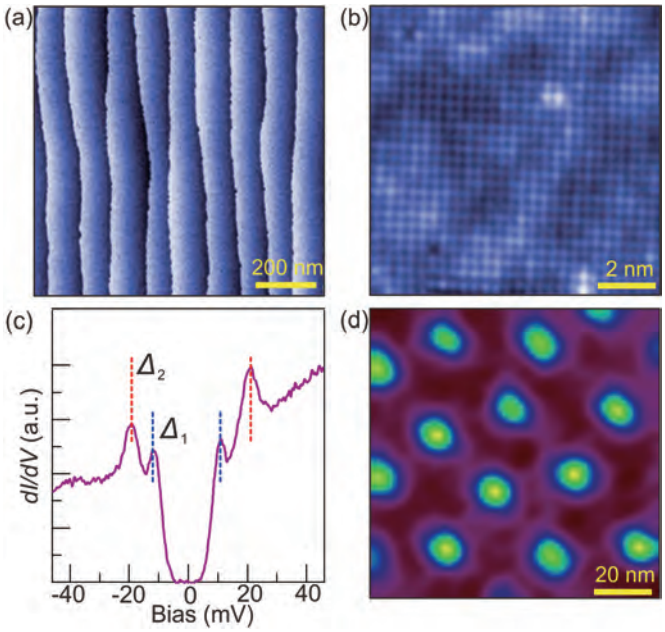

Fig. 1: (a) and (b) STM topography of 1UC-FeSe/STO(001). (c) The typical *dI/dV* spectrum ($V_s = 50$ mV, $I_t = 100$ pA) taken on the 1UC-FeSe/STO(001) at 4.2 K revealing a double-gap $\Delta_1 \sim 10$ meV and $\Delta_2 \sim 20$ meV. (d) Zero-bias conductance map ($V_s = 50$ mV, $I_t = 100$ pA) showing the vortices under a magnetic field of 11 T in 1UC-FeSe/TiO_2. (c) adapted from Wang *et al., Chin. Phys. Lett.* 29, 037402 (2012) [5], and (d) from Ding et al, *Phys. Rev. Lett.* 117, 067001 (2016) [9].

Displayed in Fig. 1(c) is a typical tunneling spectra taken on 1UC-FeSe/STO(001), showing a U-shaped double-gap structure with vanishing density of states near the Fermi energy. Two pairs of coherence peaks situate at ± 10 meV and ± 20 meV and the corresponding gaps are denoted as Δ_1 and Δ_2, respectively. Vortices occur and form an Abrikosov lattice under a magnetic field (Fig. 1(d)) as long as the 1UC-FeSe films are uniform in a large length scale ~ 50 nm [9, 27], which indicates that the large double-gap feature in 1UC-FeSe/STO(001) corresponds to remarkably enhanced superconductivity.

To summarize three features: (1) the significant promotion in superconductivity occurs as long as FeSe interfaced with $TiO_{2-\delta}$ layer, no matter the $TiO_{2-\delta}$ layers are separated by SrO or BaO layers or directly stacked layer by layer (Table 1). (2) Such a large superconducting gap is exclusively observed on the 1UC-FeSe films, while no superconducting gap is observed on 2UC and thicker films down to 4.2 K [5]. (3) The HTS in 1UC-FeSe films is independent of the ratio of Nb-doping in

Table 1. The lattice structure, magnitude of superconducting gap and gap close temperature of 1UC-FeSe films on various substrates.

	Bulk FeSe [25]	**FeSe/$SrTiO_3$**	**FeSe/TiO_2(001)**	**FeSe/$BaTiO_3$(001)** [6]
In-plane lattice (Å)	$a_0=b_0=3.765$	(001): a=b=3.80 (110): a=3.9=1.04a_0 b=3.7=0.98b_0	Anatase: a=b=3.78 Rutile: a=3.53=0.94a_0 b=3.95=1.05b_0	Relaxed: a=b=3.78 Unrelaxed: a=b=3.99=1.06a_0
Gap (meV)	2.2	(001): 16-20 [5, 14, 15] (110): 16-17 [7]	Anatase: 17-21 [9] Rutile: 14 [10]	Relaxed: 15-21 Unrelaxed: 15-21
T_{gap} (K)	9	(001): 65 [14, 26] (110): 50-60 [8, 19]	Rutile: 63±3 [10]	Relaxed: 70±2 Unrelaxed: 75±2

STO substrates [13, 26]. The above three features consistently reveal that the interface between FeSe and $TiO_{2-\delta}$ plays the key role, exactly as the case in cuprates where HTS occurs in a single CuO_2 plane interfaced with a LaSrO layer [28, 29]. Thus, we unified such interfaces as FeSe/$TiO_{2-\delta}$ interface at description of their universal properties. On the other hand, the fact that the magnitude of the superconducting gap is independent of the lattice constants (Table 1) rules out a direct correlation between the enhanced superconductivity and the strain.

Measuring the resistance of FeSe/STO(001) as a function of temperature is challenging due to its characteristics of being extremely air-sensitive and 2D limited thin - one atomic layer. We first accomplished macroscopic transport measurement on a 1UC-FeSe/STO(001) sample at a millimeter length scale after capping 10-UC FeTe as a protection layer [30]. As shown in Fig. 2(a), the resistance starts to decrease at 54.5 K and drops completely to zero at 23.5 K. Consistently, diamagnetic screening formed at 21 K (Fig. 2(b)). There are other *ex-situ* transport measurements on FeSe/STO(001) capped with either FeTe or Si protection layers revealing T_c ranging from 40 K to above 80 K [31-33]. It is worthy to note that the FeTe capping layer and the dense domain walls in 1UC-FeSe films could suppress the superconductivity in FeSe/$TiO_{2-\delta}$ [26]. Hence, the path forward to pining down the maximum T_c in FeSe/$TiO_{2-\delta}$ requires *in-situ* microscopic transport measurement. Indeed, an *in-situ* microscopic four-point probe (4PP, separated by 10-100 μm) measurement (Fig. 2(c)) gave a hint of higher T_c. Displayed in Fig. 2(d) is the I-V curves taken with the 4PP technique at various temperatures. Strikingly, zero voltage drops occur at low current and at temperatures below 109 K [34]. It is essential to conduct *in-situ* diamagnetic transport measurement to confirm the T_c value. Nevertheless, the transport results, together with spectroscopy measurements [5, 13-16, 26], verified a dramatic interfacial enhancement of T_c with respect to bulk FeSe [13]. The superconductivity enhancement in FeSe/$TiO_{2-\delta}$ is unique, for it is stronger than all the other heavily electron doped FeSe films, as will be discussed later on. Below, we discuss the Fermi surface and pairing symmetry, and essential effects (charge transfer and *e-ph* coupling) that FeSe/$TiO_{2-\delta}$ interface introduces. We emphasize that basically similar experimental results, such as electron-type Fermi surfaces, shake-off bands, etc., have been observed in FeSe/STO, FeSe/$BaTiO_3$ and FeSe/TiO_2 systems [6-10, 16, 19]. This implies universal interface effects solely introduced by the directly bounded

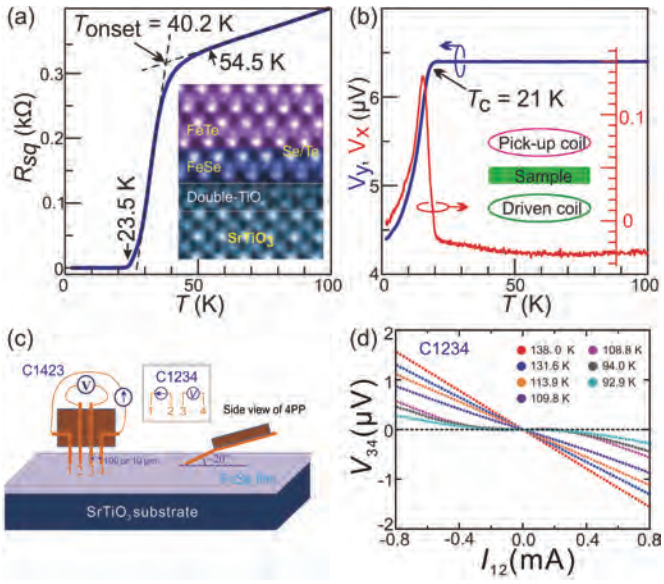

Fig. 2: (a) The temperature dependence of resistance in 1UC-FeSe/STO(001) capped by 10UC-FeTe, with the inset atomically resolved scanning transmission electron microscopy image showing the interface structure. (b) The diamagnetic response measured by a homebuilt two-coil mutual inductance system. (c) Schematic of the 4PP transport measurement set-up. (d) Typical *I–V* curves taken on 1UC-FeSe/STO(001) at various temperatures around 109 K using the setup shown in (c). (a) and (b) adapted from Zhang *et al., Chin. Phys. Lett.* 31, 017401 (2014) [30], and (c) and (d) from Ge *et al.*, Nature Mater. 14, 285 (2015) [34].

FeSe/$TiO_{2-\delta}$ interface. In the following section, we mainly show the data obtained in FeSe/STO(001), unless otherwise noted.

Fermi surface and pairing symmetry

The Fermi surface topology and pairing symmetry are two pivotal characteristics of a superconductor, considering superconductivity originates from pairing of electrons near the Fermi energy. As shown in Fig. 3(a), the Fermi surface of 1UC-FeSe films consists of only electron-like pockets centered around the Brillouin zone (BZ) corners, while the original hole pockets in the BZ center for bulk FeSe disappears completely [14-16], which indicates that 1UC-FeSe films are heavily electron doped. Very recently, high-resolution angle-resolved photo emission spectroscopy (ARPES) measurements resolved two ellipse-like electron pockets overlapping with each other at the BZ corner, e.g. the horizontal ellipse pocket δ_1 (d_{xz}/d_{yz} orbitals) and the vertical ellipse pocket δ_2 (d_{xy} orbital) shown in Fig. 3(b). With such a Fermi surface topology, superconducting gap opening occurs in each of the electron pockets. The gap values are ~ 10 meV for the δ_1 band and ~ 13 meV for the δ_2 band, agreeing with the double-gap Δ_1 ~ 10 meV and

$\Delta_2 \sim 20$ meV observed by STS (Fig. 1(c)), except for the discrepancy in the magnitude of superconducting gap Δ_2 (which varies in the range of 13-20 meV, depending on sample quality [5, 14-16]). With selective measurement on different sections of single electron pockets, both superconducting gaps are resolved to be nodeless but moderately anisotropic [35], which puts a strong constraint on the pairing symmetry. For example, as depicted in Fig. 3(c), the superconducting gap associated with the δ_2 electron pocket ranged from 8 to 13 meV in magnitude. The gap maxima are located on the δ_2 bands along the major axis of the ellipse and four gap minima are located at the intersections of δ_1 and δ_2 electron pockets, i.e. along the 45° direction of the ellipse pocket. The gap maxima location combined with the Fermi surface geometry deviate from a single d-wave, extended s-wave or $s_{\pm}$ gap function, suggesting the important role of the multiorbital nature of Fermi surfaces and orbital-dependent pairing in 1UC-FeSe/$TiO_{2-\delta}$. Meanwhile, the gap minima location may suggest possible competition between intra- and interorbital pairing [35].

Impurity scattering in superconductivity gives important information for understanding the pairing mechanism, which is usually achieved by using STM/STS via quasi-partical interference imaging (QPI) and defect imaging. For 1UC-FeSe/STO(001), phase-sensitive QPI and defect imaging consistently supports plain s-wave pairing [27]. As depicted in Fig. 4(a) and Fig. 4(b), the QPI patterns reveal scatterings between and within the electron pockets that are against line nodes. All the scattering rings exhibit overall similar suppression under magnetic fields, indicative of sign-preserving scattering here [27]. Moreover, magnetic impurities such as Cr can locally suppress the superconductivity (Fig. 4(c)), but non-magnetic impurities (Zn) do not (Fig. 4(d)). The above results suggest that 1UC-FeSe/$TiO_{2-\delta}$ has a plain *s*-wave pairing symme-

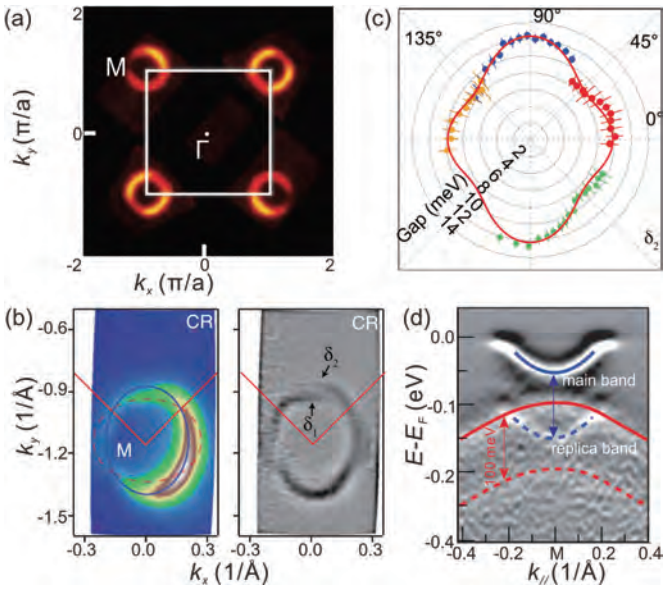

Fig. 3: (a) Integrated spectral intensity as a function of momentum for 1UC-FeSe/STO(001). (b) Fermi surface mapping (left panel) and its second derivative image (right panel) taken in circular (CR) polarization at ~ 120 K using high energy and momentum resolution. (c) Superconducting gap anisotropy on the ellipse-like electron pocket δ_2. (d) Second energy derivative of energy-momentum intensity map of 1UC-FeSe/STO(001) showing main bands and replica bands with a separation of 100 meV. (a) adapted from He *et al.*, Nat. Mater. 12, 605 (2013) [14], (b) and (c) from Zhang *et al.*, *Phys. Rev. Lett.* 117, 117001 (2016) [35], and (d) from Lee *et al.*, *Nature* 515, 245 (2014) [16].

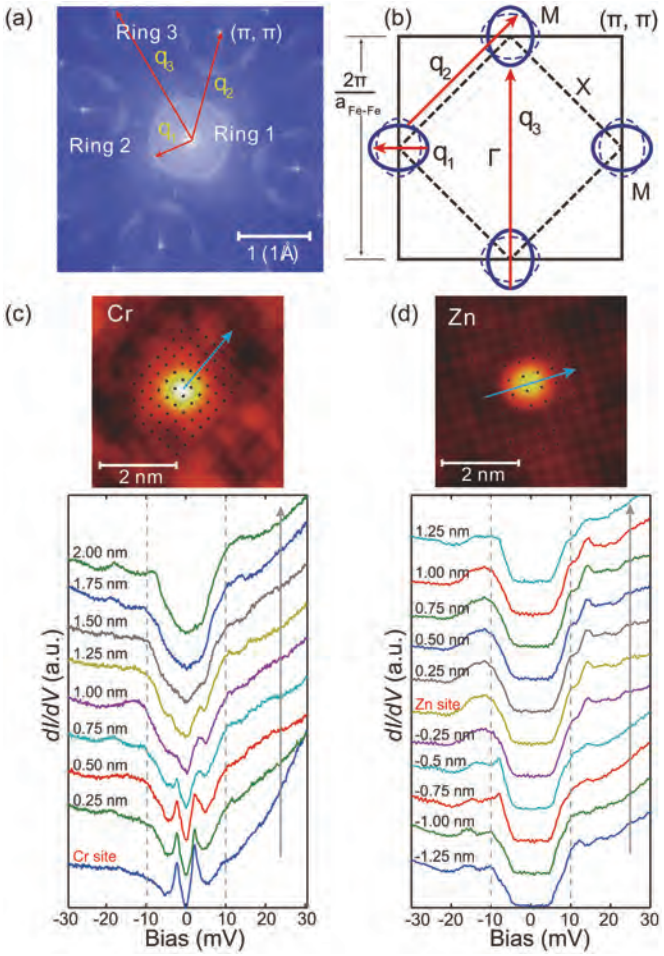

Fig. 4: (a) Fast Fourier transformation of real-space *dI/dV* maps taken at a sample bias of 22.5 meV. (b) Schematic of the BZ and Fermi surface of 1UC-FeSe/STO(001). The black solid square is the unfolded BZ with a full width of $2\pi/a_{Fe-Fe}$. The dashed square is the folded BZ. The blue solid (dashed) ellipse is the electron (folded) pocket at the M points. Red arrows mark possible scattering vectors (q_1, q_2, q_3). (c) and (d) Topographic images of Cr and Zn single adatoms and spectra taken along the arrows shown in the corresponding topographic image, respectively ($V_s = 30$ mV, $I_t = 120$ pA). Adapted from Fan *et al.*, *Nature Phys.* 11, 946 (2015) [27].

try, which is reminiscent of phonon-mediated pairing, as discussed later on.

Interface charge transfer

Extensive ARPES investigations directly characterized significant charge transfer at the FeSe/$TO_{2-\delta}$ interface, resembling that from the carrier reservoir layer to the superconducting layer in cuprates. As discussed earlier, ARPES studies showed that the Fermi surface of 1UC-FeSe/STO consists only of electron pockets at the BZ corner and there are no hole pockets at the BZ center (Fig. 3(a)), due to the interface induced charger transfer. A feature of this interface charge transfer is that the charges are mostly confined to 1UC-FeSe or the FeSe/$TiO_{2-\delta}$ interface, for the Fermi surface structure shown in Fig. 3(a) is exclusively observed on 1UC-FeSe films but not on 2UC or thicker FeSe films [15]. The doping level can reach ~ 0.12 electrons per Fe atom as derived from the Luttinger volume [14, 15]. The 2UC- and thicker FeSe films have Fermi surfaces consisting of hole pockets in the BZ center and are not superconducting [15]. Regarding the origin and mechanism of interface charge transfer, it could originate from the oxygen vacancies in the $TiO_{2-\delta}$ layers [36, 37] and/or driven by band bending at the FeSe/$TiO_{2-\delta}$ interface [38].

The interface charge transfer plays a crucial role in enhancing superconductivity in FeSe/$TiO_{2-\delta}$. Earlier promotion of T_c above 30 K with alkali metal intercalation into bulk FeSe [39] signals the remarkable superconductivity enhancement induced by electron doping. Recently, significant superconducting promotion was observed in heavily electron-doped multilayer FeSe films, where the electron doping was achieved and delicately controlled by either surface K-doping [17, 40-43] or liquid/solid gating [44-46], further confirming the prominent role of charge transfer. Taking the magnitude of the superconducting gap as the reference, the top FeSe layers with surface K adsorption exhibit maximum gaps of 10-13 meV [17, 40-43], between those of bulk FeSe and FeSe/$TiO_{2-\delta}$. As shown in Fig. 5(a) are the dI/dV spectra taken on FeSe films grown on graphene with optimal surface K-doping (roughly 0.25 monolayer (ML) K). With the exception that K-coated 1UC-FeSe exhibits a smaller gap ~ 6.6 meV due to stronger suppression induced by thermal/quantum fluctuation in 2D limit, all others exhibit identical double-gap Δ_1 ~ 10 meV and Δ_2 ~ 13 meV. This indicates a HTS phase of heavily electron-doped FeSe films with respect to bulk FeSe, but the magnitude of Δ_2 is smaller than that of FeSe/$TiO_{2-\delta}$. More specifically, the HTS phase emerges abruptly at a K coverage of 0.103 ML, while the native superconductivity in bulk FeSe with a characterized superconducting gap Δ_s ~ 2.2 meV weakens first with K adsorption and finally vanishes entirely at a K coverage of 0.033 ML (Fig. 5(b)). Subsequent ARPES investigation reveals that such superconductivity evolution accompanies Liftshitz transitions of Fermi surface and variation in correlation strength with increasing doping [43]. Taking T_c as reference, the heavily electron-doped FeSe films where electrons are injected by using liquid gating technique showed maximum T_c around 40 K [44-46], again between those of bulk FeSe and FeSe/$TiO_{2-\delta}$.

Charge transfer does promote a HTS phase in electron-doped FeSe, however, it alone cannot account for the full superconductivity enhancement in FeSe/$TiO_{2-\delta}$, which has a larger superconducting gap and higher T_c than all the other heavily electron doped FeSe [5, 9, 17, 45, 46]. That is, the FeSe/$TiO_{2-\delta}$ interface introduces additional novel effects beyond doping. Refined STS studies indicate that the additional enhancement decays exponentially with the FeSe layer moving away from $TiO_{2-\delta}$ layer [17, 42]. Displayed in Fig. 5(c) is the typical dI/dV curves taken on 1-4 UC FeSe/STO(001) at optimal doping of ~ 0.12 electrons per Fe atom. The transferred charges for the topmost layer of 2-4 UC films are from surface K and those for 1UC films are from the bottom $TiO_{2-\delta}$

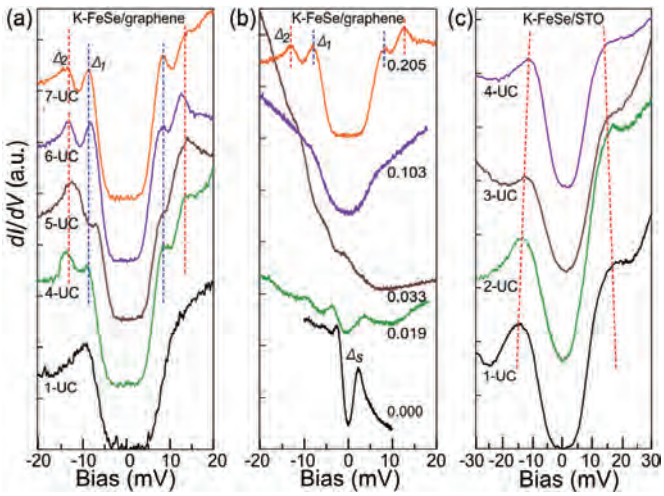

Fig. 5: (a) *dI/dV* spectra (V_s = 30 mV, I_t = 100 pA) taken on FeSe films with various thicknesses and optimal surface K doping on graphene. (b) *dI/dV* spectra (V_s = 20 mV, I_t = 100 pA) taken on multilayer FeSe films on graphene with various K coverage, as indicated. (c) *dI/dV* spectra (V_s = 30 mV, I_t = 100 pA) taken on 1-4 UC FeSe films on STO(001) at optimal doping. The dashes are guide for eyes, showing the change of coherence peaks. (a) and (b) adapted from Song *et al., Phys. Rev. Lett.* 116, 157001 (2016) [41], and (c) from Tang *et al., Phys. Rev. B* 93, 020507 (2016) [17].

layer. Clearly, the superconducting gap decays as the thickness increases from 1UC to 4 UC (Fig. 5(c)). It is an exponential decay with a decay length of 2.4 UC [42]. Beyond 4 UC, the superconducting gap of optimal doped FeSe films on STO doesn't change with increasing thickness and remains at a constant value [42], agreeing with the thickness-independent superconducting gap in electron-doped FeSe films on graphene (with the only exception of 1UC-FeSe/graphene, due to strong fluctuation and without the interface enhance effect) [41]. The contrast in Fig. 5(a) and 5(c) confirms that FeSe/$TiO_{2-\delta}$ interface does contribute additional novel effects instead of doping even for 2-3 UC FeSe films.

Interface enhanced *e-ph* coupling

Interface enhanced *e-ph* coupling was proposed as a key factor when a large superconducting gap of 20 meV in FeSe/STO system was first reported [5]. Indeed, the subsequent ARPES, STS, ultrafast optical spectroscopy and high-resolution electron energy loss spectroscopy (HREELS) investigations successively identified the interface enhanced *e-ph* coupling and its correlation with the HTS [16-18, 47], which is also theoretically supported [16, 20, 22]. This interface enhanced *e-ph* coupling could include two parts. One is the interfacial coupling between FeSe electrons and oxygen optical phonons in STO. This was first suggested by ARPES observations of replica bands with energy separation of ~ 100 meV (Fig. 3(d)), which is a feature of coupling between oxygen optical phonons in STO at such frequency and FeSe electrons. It was further revealed by surface-sensitive phonon investigations using HREELS [18]. As exhibited in the energy distribution curves taken on FeSe/STO with different FeSe thicknesses shown in Fig. 6(b), the electric field generated by Fuchs-Kliewer (F-K) phonons (α and β modes shown in Fig. 6(a) with energy of 92 meV and 60 meV, respectively) in STO penetrate into the epitaxial FeSe films. This penetration guarantees the interaction between the electrons in FeSe films and the STO phonons. More importantly, the electric field generated by these F-K phonons decays exponentially with a decay length of 2.5 UC FeSe (Fig. 6(b) and 6(c)), consistent with the unique exponential decay of the superconducting gap in K-coated (1-4)UC-FeSe/STO shown in Fig. 5(c). This consistent decay behavior, i.e. exponential decay with same decay length (Fig. 6(c)), suggests the contribution of these F-K phonons to the additional enhanced superconductivity beyond doping. The α mode shown in Fig. 6(a), mainly due to relative Ti and O atomic displacement along the [001] direction, agrees with the phonon mode deduced from the ARPES resolved shake-off bands (Fig. 3(d)) in energy, i.e. 92 meV vs. 100 meV. First principles calculations also verified the further enhancement in pairing strength induced by such interfacial *e-ph* coupling despite the paring mechanism [22, 23].

The other part is enhanced *e-ph* coupling in the epitaxial FeSe films, which contributes to the HTS as well. STO substrates act as a template, stabilizing the structure in the epitaxial 1UC-FeSe films and ruining nematic order in bulk FeSe [43]. As a result of this substrate-bound structure, two *e-ph* coupling channels with phonon frequencies of ~ 10 meV and ~ 20 meV open [20]. The two phonon modes are clearly resolved as two pairs of dip-hump features in the tunneling spectra at energies of ± (Δ+Ω) (Fig. 6(d)), where Ω_1 ~ 11 meV and Ω_2 ~ 19 meV,

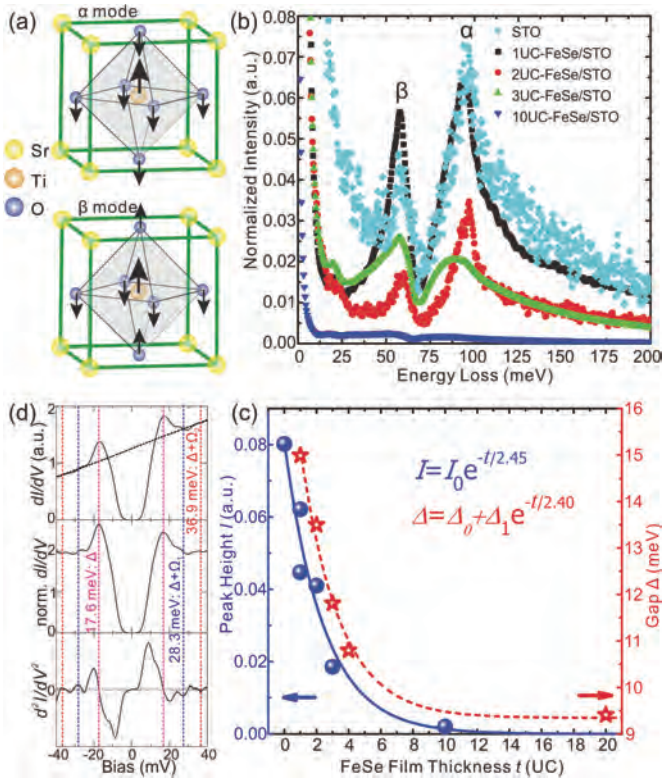

Fig. 6: (a) Ionic vibrations of the α and β modes of STO. (b) Energy distribution curves at the Γ point for 1-3UC- and 10UC-FeSe films on STO(001). (c) Plot and exponential fitting of the peak height of α mode as a function of the FeSe thickness (blue). Plot and exponential fitting of the superconducting gap size for the K-doped FeSe/STO(001) as a function of the FeSe thickness (red), with data extracted from Ref [42]. (d) Typical *dI/dV* (top panel, V_s = 50 mV, I_t = 100 pA), normalized *dI/dV* (middle panel), and d^2I/dV^2 (bottom panel) spectra taken on bare 1UC-FeSe/STO(001). The pink, blue and red dashes show the approximate energy positions of ± Δ, ± (Δ + Ω_1) and ± (Δ + Ω_2), respectively. (a)-(c) adapted from Zhang *et al.*, *Phys. Rev. B* 94, 081116 (2016) [18], and (d) from Tang *et al.*, *Phys. Rev. B* 93, 020507 (2016) [17].

consistent with the E_g(Se) and A_{1g}(Se) phonons of FeSe in energy [17]. They accompany the superconducting gap, remain in identical energy irrespective of the magnitude of superconducting gap (i.e. independent of doping level), but degrade simultaneously with increasing temperature as superconducting gaps do [17]. The above behaviors attest to their origin by *e-ph* coupling and their correlation with superconductivity. ARPES investigations with femtosecond time resolution also identified a phonon mode $\Omega_2 \sim 21$ meV that becomes soft at the FeSe/STO interface [48]. In contrast, for FeSe films grown on and weakly bonded to graphene, although a bosonic mode occurs, the energy is quite low as in a level of 2.7-4 meV [49]. The sharp contrast proves the special role of the STO substrate in boosting the *e-ph* coupling and hence creating further enhanced superconductivity beyond doping.

CONCLUSION

The observation of remarkable enlarged superconducting gap and enhanced T_c in 1UC-FeSe on various $TiO_{2-\delta}$ terminated substrates, such as STO, $BaTiO_3$ and TiO_2, demonstrates that interface engineering provides a feasible way for rational design and preparation of high-T_c superconductors. Motivated by such discoveries, an idea comes naturally to mind; that is, to search for an even higher T_c by fabricating a sandwiched heterostructure of FeSe bonded to $TiO_{2-\delta}$ on both sides and hence taking advantage of doubled interface enhancement. The first principle calculations on the structural stability and electronic structure confirms the validity of such a double-interface enhancement [50]. Regarding the crucial role that the interface plays, it includes interface charge transfer and interface enhanced *e-ph* coupling. In terms of the resemblance between the FeSe/$TiO_{2-\delta}$ interface and the built in multi-interface structures in cuprate and iron pnictide superconductors, understanding the interfacial high-T_c in FeSe/$TiO_{2-\delta}$ provides clues to deciphering the mysterious high-T_c superconductivity in cuprates. The essential role of interface charge doping (similar to modulation-doping [4, 51]) has been generally accepted, and furthermore, the contribution of oxygen phonons, as evidenced in both FeSe/$TiO_{2-\delta}$ [16, 18] and cuprates [52, 53], deserves to be revisited. Further exploration of interface superconductivity is a promising avenue for raising T_c, as well as for understanding the mechanism of HTS.

Acknowledgements: The authors gratefully acknowledge the collaborations and discussions with Xun-Cun Ma, Jin-Feng Jia, Can-Li Song, Xingjiang Zhou, Jian Wang, Ji-Min Zhao, Yayu Wang, Lin Gu, Mingwei Chen, Dung-Hai Lee, Shengbai Zhang, Fuchun Zhang, and Xincheng Xie. This work was supported by the National Nature Science Foundation of China and the National Basic Research Program of China.

References

[1] H. K. Onnes, Leiden Comm. 120b, 122b, 124c (1911).
[2] J. G. Bednorz and K. A. Müller, Z. Phys. B 64, 189 (1986).
[3] Y. Kamihara, T. Watanabe, M. Hirano, and H. Hosono, J. Am. Chem. Soc. 130, 3296 (2008).
[4] R. Dingle, H. L. Störmer, A. C. Gossard, and W. Wiegmann, Appl. Phys. Lett. 33, 665 (1978).
[5] Q.-Y. Wang, Z. Li, W.-H. Zhang, Z.-C. Zhang, J.-S. Zhang, W. Li, H. Ding, Y.-B. Ou, P. Deng, K. Chang, J. Wen, C.-L. Song, K. He, J.-F. Jia, S.-H. Ji, Y.-Y. Wang, L.-L. Wang, X. Chen, X.-C. Ma, and Q.-K. Xue, Chin. Phys. Lett. 29, 037402 (2012).
[6] R. Peng, H. C. Xu, S. Y. Tan, H. Y. Cao, M. Xia, X. P. Shen, Z. C. Huang, C. H. Wen, Q. Song, T. Zhang, B. P. Xie, X. G. Gong, and D. L. Feng, Nature Commun. 5, 5044 (2014).
[7] G. Zhou, D. Zhang, C. Liu, C. Tang, XiaoxiaoWang, Z. Li, C. Song, S. Ji, K. He, L.-L. Wang, X.-C. Ma, and Q.-K. Xue, Appl. Phys. Lett. 108, 202603 (2016).
[8] P. Zhang, X. L. Peng, T. Qian, P. Richard, X. Shi, J. Z. Ma, B. B. Fu, Y. L. Guo, Z. Q. Han, S. C. Wang, L.-L. Wang, Q. K. Xue, J. P. Hu, Y. J. Sun, and H. Ding, Phys. Rev. B 94 (2016).
[9] H. Ding, Y. F. Lv, K. Zhao, W. L. Wang, L.-L. Wang, C. L. Song, X. Chen, X. C. Ma, and Q. K. Xue, Phys. Rev. Lett. 117, 067001 (2016).
[10] S. N. Rebec, T. Jia, C. Zhang, M. Hashimoto, D.-H. Lu, R. G. Moore, and Z.-X. Shen, Phys. Rev. Lett. 118, 067002 (2017).
[11] C. W. Chu, L. Z. Deng, and B. Lv, Physica C 514, 290 (2015).
[12] G. R. Stewart, Rev. Mod. Phys. 83, 1589 (2011).
[13] L.-L. Wang, X.-C. Ma, and Q.-K. Xue, Supercond. Sci. Technol. 29, 123001 (2016).
[14] S. He, J. He, W. Zhang, L. Zhao, D. Liu, X. Liu, D. Mou, Y. B. Ou, Q. Y. Wang, Z. Li, L.-L. Wang, Y. Peng, Y. Liu, C. Chen, L. Yu, G. Liu, X. Dong, J. Zhang, C. Chen, Z. Xu, X. Chen, X.-C. Ma, Q.-K. Xue, and X. J. Zhou, Nature Mater. 12, 605 (2013).
[15] S. Tan, Y. Zhang, M. Xia, Z. Ye, F. Chen, X. Xie, R. Peng, D. Xu, Q. Fan, H. Xu, J. Jiang, T. Zhang, X. Lai, T. Xiang, J. Hu, B. Xie, and D. Feng, Nature Mater. 12, 634 (2013).
[16] J. J. Lee, F. T. Schmitt, R. G. Moore, S. Johnston, Y. T. Cui, W. Li, M. Yi, Z. K. Liu, M. Hashimoto, Y. Zhang, D. H. Lu, T. P. Devereaux, D. H. Lee, and Z. X. Shen, Nature 515, 245 (2014).
[17] C. Tang, C. Liu, G. Zhou, F. Li, H. Ding, Z. Li, D. Zhang, Z. Li, C. Song, S. Ji, K. He, L.-L. Wang, X.-C. Ma, and Q.-K. Xue, Phys. Rev. B 93, 020507 (2016).
[18] S. Zhang, J. Guan, X. Jia, B. Liu, W. Wang, F. Li, L.-L. Wang, X.-C. Ma, Q.-K. Xue, J. Zhang, E. W. Plummer, X. Zhu, and J. Guo, Phys. Rev. B 94, 081116 (2016).
[19] C. Zhang, Z. Liu, Z. Chen, Y. Xie, R. He, S. Tang, J. He, W. Li, T. Jia, S. N. Rebec, E. Y. Ma, H. Yan, M. Hashimoto, D. Lu, S.-K. Mo, Y. Hikita, R. G. Moore, H. Y. Hwang, D. Lee, and Z. Shen, Nature Commun. 8, 14468 (2017).
[20] S. Coh, M. L. Cohen, and S. G. Louie, New J. Phys. 17, 073027 (2015).
[21] Y. Xie, H. Y. Cao, Y. Zhou, S. Chen, H. Xiang, and X. G. Gong, Sci. Rep. 5, 10011 (2015).
[22] Y. Wang, A. Linscheid, T. Berlijn, and S. Johnston, Phys. Rev. B 93, 134513 (2016).

[23] Z. X. Li, F. Wang, H. Yao, and D. H. Lee, Sci. Bul. 61, 925 (2016).
[24] F. C. Hsu, J. Y. Luo, K. W. Yeh, T. K. Chen, T. W. Huang, P. M. Wu, Y. C. Lee, Y. L. Huang, Y. Y. Chu, D. C. Yan, and M. K. Wu, Proc. Natl. Acad. Sci. USA 105, 14262 (2008).
[25] C.-L. Song, Y.-L. Wang, Y.-P. Jiang, Z. Li, L.-L. Wang, K. He, X. Chen, X.-C. Ma, and Q.-K. Xue, Phys. Rev. B 84, 020503 (2011).
[26] W. Zhang, Z. Li, F. Li, H. Zhang, J. Peng, C. Tang, Q. Wang, K. He, X. Chen, L.-L. Wang, X.-C. Ma, and Q.-K. Xue, Phys. Rev. B 89, 060506 (2014).
[27] Q. Fan, W. H. Zhang, X. Liu, Y. J. Yan, M. Q. Ren, R. Peng, H. C. Xu, B. P. Xie, J. P. Hu, T. Zhang, and D. L. Feng, Nature Phys. 11, 946 (2015).
[28] D. Jiang, T. Hu, L. You, A. L. Qiao Li1, H. Wang, G. Mu, Z. Chen, H. Zhang, G. Yu, J. Zhu, Q. Sun, C. Lin, H. Xiao, X. Xie, and M. Jiang, Nature Commun. 5, 5708 (2014).
[29] G. Logvenov, A. Gozar, and I. Bozovic, Science 326, 699 (2009).
[30] W.-H. Zhang, Y. Sun, J.-S. Zhang, F.-S. Li, M.-H. Guo, Y.-F. Zhao, H.-M. Zhang, J.-P. Peng, Y. Xing, H.-C. Wang, T. Fujita, A. Hirata, Z. Li, H. Ding, C.-J. Tang, M. Wang, Q.-Y. Wang, K. He, S.-H. Ji, X. Chen, J.-F. Wang, Z.-C. Xia, L. Li, Y.-Y. Wang, J. Wang, L.-L. Wang, M.-W. Chen, Q.-K. Xue, and X.-C. Ma, Chin. Phys. Lett. 31, 017401 (2014).
[31] Y. Sun, W. Zhang, Y. Xing, F. Li, Y. Zhao, Z. Xia, L.-L. Wang, X.-C. Ma, Q.- K. Xue, and J. Wang, Sci. Rep. 4, 6040 (2014).
[32] L. Z. Deng, B. Lv, Z. Wu, Y. Y. Xue, W. H. Zhang, F. S. Li, L.-L. Wang, X.-C. Ma, Q.-K. Xue, and C. W. Chu, Phys. Rev. B 90 (2014).
[33] Z. Zhang, Y.-H. Wang, Q. Song, C. Liu, R. Peng, K. A. Moler, D. Feng, and Y. Wang, Sci. Bull. 60, 1301 (2015).
[34] J. F. Ge, Z. L. Liu, C. Liu, C. L. Gao, D. Qian, Q.-K. Xue, Y. Liu, and J. F. Jia, Nature Mater. 14, 285 (2015).
[35] Y. Zhang, J. J. Lee, R. G. Moore, W. Li, M. Yi, M. Hashimoto, D. H. Lu, T. P. Devereaux, D. H. Lee, and Z. X. Shen, Phys. Rev. Lett. 117, 117001 (2016).
[36] J. Bang, Z. Li, Y. Y. Sun, A. Samanta, Y. Y. Zhang, W. Zhang, L.-L. Wang, X. Chen, X.-C. Ma, Q.-K. Xue, and S. B. Zhang, Phys. Rev. B 87, 220503 (2013).
[37] F. Li, Q. Zhang, C. Tang, C. Liu, J. Shi, C. Nie, G. Zhou, Z. Li, W. Zhang, C.-L. Song, K. He, S. Ji, S. Zhang, L. Gu, L.-L. Wang, X.-C. Ma, and Q.-K. Xue, 2D Mater. 3, 024002 (2016).
[38] H. Zhang, D. Zhang, X. Lu, C. Liu, G. Zhou, X.-C. Ma, L.-L. Wang, P. Jiang, Q.-K. Xue, and X. Bao, Nature Commun. accepted (2017).
[39] J. Guo, S. Jin, GangWang, ShunchongWang, K. Zhu, T. Zhou, M. He, and X. Chen, Phys. Rev. B 82, 180520 (2010).
[40] Y. Miyata, K. Nakayama, K. Sugawara, T. Sato, and T. Takahashi, Nature Mater. 14, 775 (2015).
[41] C.-L. Song, H. M. Zhang, Y. Zhong, X. P. Hu, S. H. Ji, L.-L. Wang, K. He, X.-C. Ma, and Q.-K. Xue, Phys. Rev. Lett. 116, 157001 (2016).
[42] W. H. Zhang, X. Liu, C. H. Wen, R. Peng, S. Y. Tan, B. P. Xie, T. Zhang, and D. L. Feng, Nano Lett. 16, 1969 (2016).
[43] C. H. Wen, H. C. Xu, C. Chen, Z. C. Huang, X. Lou, Y. J. Pu, Q. Song, B. P. Xie, M. Abdel-Hafiez, D. A. Chareev, A. N. Vasiliev, R. Peng, and D. L. Feng, Nature Commun. 7, 10840 (2016).
[44] J. Shiogai, Y. Ito, T. Mitsuhashi, T. Nojima, and A. Tsukazaki, Nature Phys. 12, 42 (2015).
[45] B. Lei, J. H. Cui, Z. J. Xiang, C. Shang, N. Z. Wang, G. J. Ye, X. G. Luo, T. Wu, Z. Sun, and X. H. Chen, Phys. Rev. Lett. 116, 077002 (2016).
[46] K. Hanzawa, H. Sato, H. Hiramatsu, T. Kamiya, and H. Hosono, Proc. Natl. Acad. Sci. USA 113, 3986 (2016).
[47] Y. C. Tian, W. H. Zhang, F. S. Li, Y. L. Wu, Q. Wu, F. Sun, G. Y. Zhou, L. -L. Wang, X.-C. Ma, Q.-K. Xue, and J. Zhao, Phys Rev Lett 116, 107001 (2016).
[48] S. Yang, J. A. Sobota, D. Leuenberger, A. F. Kemper, J. J. Lee, F. T. Schmitt, W. Li, R. G. Moore, P. S. Kirchmann, and Z. X. Shen, Nano Lett. 15, 4150 (2015).
[49] C.-L. Song, Y.-L. Wang, Y.-P. Jiang, Z. Li, L.-L. Wang, K. He, X. Chen, J. E. Hoffman, X.-C. Ma, and Q.-K. Xue, Phys. Rev. Lett. 112, 057002 (2014).
[50] S. Coh, D.-H. Lee, S. G. Louie, and M. L. Cohen, Phys. Rev. B 93 (2016).
[51] Y. Zhong, Y. Wang, S. Han, Y.-F. Lv, W.-L. Wang, D. Zhang, H. Ding, Y.-M. Zhang, L.-L. Wang, K. He, R. Zhong, J. A. Schneeloch, G.-D. Gu, C.-L. Song, X.-C. Ma, and Q.-K. Xue, Sci. Bull. 61, 1239 (2016).
[52] A. Lanzara, P. V. Bogdanov, X. J. Zhou, S. A. Kellar, D. L. Feng, E. D. Lu, T. Yoshida, H. Eisaki, A. Fujimori, K. Kishio, J.-I. Shimoyama, T. Noda, S. Uchida, Z. Hussain, and Z.-X. Shen, Nature 412, 510 (2001).
[53] D. Reznik, L. Pintschovius, M. Ito, S. Iikubo, M. Sato, H. Goka, M. Fujita, K. Yamada, G. D. Gu, and J. M. Tranquada, Nature 440, 1170 (2006).

Lili Wang is an associate professor at Tsinghua University, China. After receiving her PhD degree in physics from the Institute of Physics, Chinese Academy of Sciences (IOP, CAS) in 2006, she worked at Rice University as a postdoctoral researcher from 2006 to 2008. She joined in IOP, CAS in 2008 and then the Department of Physics, Tsinghua University in 2013. Her research focuses on novel properties of low dimensional quantum materials.

Qi-Kun Xue is a distinguished professor of Tsinghua University, China and an academician of the Chinese Academy of Sciences. After receiving a PhD degree from the Institute of Physics, Chinese Academy of Sciences (IOP, CAS) in 1994, he worked at Tohoku University, North Carolina State University, and IOP, CAS before joining Tsinghua University in 2005. His current research focuses on low dimensional quantum materials, including superconductors and topological insulators. His group pioneered the experimental research of quantum anomalous Hall effect and interface high temperature superconductivity.